Journal of Sustainable Metallurgy (2019) 5:482–496
https://doi.org/10.1007/s40831-019-00236-8

RESEARCH ARTICLE

Chemical Composition Simplification of the Seydişehir (Konya, Turkey) Alumina Plant Waste

Tuğba Selcen Atalay Kalsen[1] · Hakan Burak Karadağ[1] · Yasin Ramazan Eker[1] · Işıl Kerti[2]

Received: 4 March 2019 / Revised: 26 June 2019 / Accepted: 28 June 2019 / Published online: 31 July 2019
© The Minerals, Metals & Materials Society 2019

Abstract

Red mud, a residue of alumina production from bauxite refining, contains oxides of valuable metals such as Fe, Al, Ti, Si, Na, Ca, etc. The presence of these numerous metal oxides does not allow introducing the highly basic raw red mud within any industrial process, which leads to its storage over a wide land area. In order to simplify the chemical composition of this waste, the effects of weak acid leaching (citric acid) and strong acid leaching (hydrochloric acid) are studied. The treatment efficiency is discussed based on scanning electron microscope and X-ray diffraction analysis of solid product and inductively coupled plasma spectrometry analysis of acidic solutions. The effects of temperature and acid concentration on metals dissolution are estimated by rough kinetic considerations which present results comparable to those in the literature. More than 50% of Al and 50% of Ca detected by inductively coupled plasma mass spectrometry were separated via the organic acid process, while during leaching with HCl whole Ca, Fe, and more than 60% Ti and 80% of Al similarly determined were recovered. This confirms that within the red mud, metals behave differently under several forms with different reactivity toward acidic medium. Therefore, an eventual combination of both acids can be an efficient way to prepare them ready and suitable for possible industrial applications.

Keywords Metal leaching · Citric acid · Red mud · Hydrochloric acid

Introduction

Bauxite is the main raw material used for aluminum production in the Bayer chemical process. The first step of this process is to digest the ore with sodium hydroxide (NaOH) under heat and pressure. At the end of this step, the produced red mud and aluminum hydroxide are separated. Depending on the bauxite characteristics, about 1.5–2.5 tons of red mud per ton of produced alumina are continuously generated around the world [1, 2]. These alkaline (pH 10–12.5) wastes mainly consisting of stable oxides cause environmental damage and groundwater pollution. Unfortunately, industrialists are forced to dispose this waste in natural surrounding areas since no sustainable recovery solution has been developed [3, 4].

The red mud composition is affected by the origin of bauxite mineral, as well as the Bayer process parameters (temperature, pressure, time, etc.). The main solution suggested to valorize red mud is to directly integrate the wastes in different applications, such as ceramics additive, catalyst, or heavy metal adsorbent [5–7]. However, the complex content of waste prevents optimization of the performance and implies the need for the extraction of the selected elements from the residue before their use. One of the suggested solutions is to recover metals and rare earths present in red muds by means of hydrometallurgical, pyrometallurgical, or hybrid techniques. Unfortunately, none of them are sufficiently economically viable for an industrial application; moreover, these processes can originate extra contaminant produced during the recovery [8–11].

There are hydrometallurgical studies on the recovery of metals using red mud samples originating from the bauxite mine-rich regions in the world, such as Australia (24.4%), Greece (2.6%), China (1.7%), and Hungary (1.3%) [12]. The leaching process of Australian red mud with strong

The contributing editor for this article was Brajendra Mishra.

✉ Yasin Ramazan Eker
yeker@erbakan.edu.tr

[1] Metallurgical and Materials Engineering Department, Necmettin Erbakan University, Konya, Turkey

[2] Metallurgical and Materials Engineering Department, Yıldız Technical University, Istanbul, Turkey

acids (e.g., nitric, hydrochloric, sulfuric, and phosphoric) leads to different recovery performances. Unselective or indiscriminate leaching products of overall metals are obtained with hydrochloric acids, involving subsequently a complex separation step of the metal ions in solution. The maximum total dissolution of leached metals is at about 60%, with almost 50% for Al being obtained with 1.25:1000 solid:solution ratio by leaching with 1 M phosphoric acid after 24 h of leaching at 25 °C. In the former conditions, the iron recovery is only ~ 6%. Upon increasing the phosphoric acid concentration to 5 M at 25 °C (24 h, 5:1000 solid:solution ratio), the iron recovery is about 50%. On the other hand, in the presence of sulfuric acid (1 M, 80 °C, 5:1000 solid:solution ratio), the total dissolution yield is only ~ 40%. Under the same conditions, the maximum titanium dissolution rate is ~ 10% in phosphoric acid, while it does not exceed 20% in sulfuric acid. Finally, the dissolution efficiencies for Al and Si within nitric acid are comparable to those within phosphoric acid, while they are lower especially for Fe (~ 6%) and Ti (~ 10%) [12]. Concerning the Greek red mud, a different leaching performance was obtained for iron (80%) when using nitric acid [13]. The chemical analysis showed that, in the Australian red mud, the iron was only derived from hematite (Fe_2O_3), while hematite and goethite [FeO(OH)] are found to be mixed together within the Greek red mud. This difference can be explained by taking the original constitution of the bauxite mineral into consideration or by a possible transformation taking place during the aluminum extraction process. Therefore, the selective metal extraction process seems to be dependent on the mineral type within the residue.

The leaching process is not specific to strong acids, and it can also be performed using organic acids like citric acid (*2-hydroxypropane-1,2,3-tricarboxylic acid*), for example (Fig. 1) [14–19]. Thus, the leaching of Indonesian saprolitic ore bearing goethite and serpentine minerals is possible with different inorganic (e.g., HCl, H_2SO_4, HNO_3) and organic (e.g., citric, lactic, oxalic acid) acid mediums [14]. 45% Ni leaching efficiency was obtained with HCl and HNO_3 solutions, while Fe was highly dissolved in sulfuric acid solution for a leaching time of 7 days at 30 °C. Under the same conditions, 72% Ni is leached out from the ore with 1 M citric acid solution. In addition, the X-ray diffraction (XRD) data of leaching residues show that the acid performs leaching selectively since the dissolved part of Ni with citric acid was not associated to the goethite phase. In fact, citric acid contains three acid functions with three different $pKa_1 = 3.13$, $pKa_2 = 4.76$, and $pKa_3 = 6.40$ allowing it to be a polydentate ligand [20]. Compared with the other typical carboxylic acids, it is slightly stronger due to the anion stabilization by the intramolecular hydrogen bonding from the other protic groups within its structure. Therefore, this weak acid can dissolve heavy metals either by direct displacement of metal ions with hydrogen ions or by forming soluble metal complexes/chelates [15, 21].

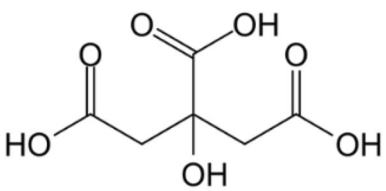


Fig. 1 Chemical structure of citric acid

In addition, citric acid can be used as an additive to improve the leaching yield of 5 M sulfuric acid. By adding 5% citric acid with a liquid-to-solid ratio of 5:1 at 90 °C for 60 min, amounts of 82% of Ti, 66% of V, 78% of Fe, and 71% of Al have been recovered from China red mud [22]. The effect of citric acid is indubitable; however, the selectivity is once again neglected, and the recovery process will require additional complex steps.

This work aims to evaluate the leaching behavior of metals in red mud from Seydişehir Aluminium Plant using separately a citric acid medium and hydrochloric acid medium. The leaching parameters (leaching time, acid concentration, and leaching temperature) have been investigated for both media in order to reach the maximum selectivity. Finally, a combination of the most efficient treatments has been theoretically suggested in order to yield the purest product ready and compatible for industrial use.

Materials and Methods

Leaching tests were carried out in boiling flasks by refluxing within oil bath using magnetic stirrer at a constant speed of 300 rpm. For the preparation of a citric acid solution, 10 g, 30 g, and 50 g sour salt bought in the market as E330 were dissolved in 50 mL distilled water, while the HCl solutions (1, 4, and 8 mol/L) were prepared from HCl (Merck 37%). Leaching solutions were prepared in order to get a total volume of 50 mL including 5 g red mud, which involves solutions with 100 g/L pulp density. The effect of leaching time was investigated by holding within the leaching media for 1, 3, and 5 h. All time-independent experiments have been done at 25 °C. Concerning the investigation of the temperature effect, tests were carried out at 25 °C, 50 °C, and 100 °C for 3 h. Metal contents in pregnant leaching solutions were measured by inductively coupled plasma mass spectrometry (ICP-MS; Thermo Scientific iCAP 7000 Series), and leaching efficiencies were calculated by the following equation:

$$\text{Metal extraction (\%)} = \frac{\text{Metal concentration in leachate (g/L)}}{\text{Total metal concentration in red mud (g/L)}} \times 100. \quad (1)$$

The sour salt has been characterized via Raman analysis (Renishaw InVia Reflex, laser 532 nm), and the comparison with spectra of analytical solid citric acid (Sigma Aldrich 99%) confirms that both samples have the same chemical structure (Fig. 2). However, peaks of sour salt are broader and peaks' intensities at about 3000 cm^{-1} are higher compared with the other peaks. This suggests that the sour salt consists in hydrated citric acid as described in the literature [23]: *Spectral Database for Organic Compounds SDBS* (*565 and 1995*).

Results and Discussion

Characterization of Raw Materials

In Seydişehir Aluminum Production Plant, bauxite ore is first crushed and wet ground with NaOH at 100 °C, thus yielding the pulp. The former is treated with NaOH (26%) under water vapor (~440 °C) and 46 bar pressure. During the cooling down process when the temperature of the caustisized pulp reaches about 250 °C, the solution is filtered. This leads to the separation of the solid phase called red mud and the aqueous phase consisting of sodium aluminate within the caustic solution. Moreover, due to the activation of silicon materials within the basic medium, sodium silicate components are precipitates and are present within the final solid waste.

The red mud that is dried, crushed, and sieved to size fractions under 500 µm is analyzed via X-ray fluorescence (XRF; by ACME Analytical Laboratories, Canada) for determining the accurate chemical content, and characterized via XRD spectroscopy (Bruker D8 Advance, Cu Kα) for determining the structure of the present crystals. Thereafter, the thermal stability of the sample has been examined by means of thermal gravimetric analysis (TGA) (LABSYS Evo). Finally, the scanning electron microscopy coupled with electron dispersive spectroscopy (SEM–EDX; Hitachi SU1510, Oxford X-Act) has been used to obtain the information concerning the particles' morphology (20 kV, × 1000) and the chemical elemental distribution within the sample.

Since red mud is the product resulting from the highly basic process (Bayer process), the XRF analysis has been done by considering the metals. The distributions in masses of these elements are shown in Table 1. The predominantly present element is Fe giving to the sample its red color (and thus its name), while the presence of Al proves that the Bayer process is not wholly efficient for aluminum recovery. Finally, the caustic treatment at the beginning of the process is the reason of the presence of Na within the waste.

The XRD analysis of the red mud (Fig. 3) gives more accurate information concerning the crystalline phase of the oxides detected by XRF. The highest peaks on diffractogram belong to the hematite (Fe_2O_3) indicating that hematite is the main Fe component. On the other hand, Al is principally due to the gibbsite [$Al(OH)_3$], but also diaspore [AlO(OH)] and cancrinite [$Na_8Al_6Si_6O_{24}(CO_3)(H_2O)_2$] which is a feldspathoid. Otherwise, Si is also present in quartz (SiO_2) form. Finally, Ca and Ti are respectively detected as calcite

Table 1 Main elemental composition of red mud

Element	Wt%
Fe	29.72
Al	10.79
Si	7.47
Na	7.72
Ti	3.46
Ca	1.01

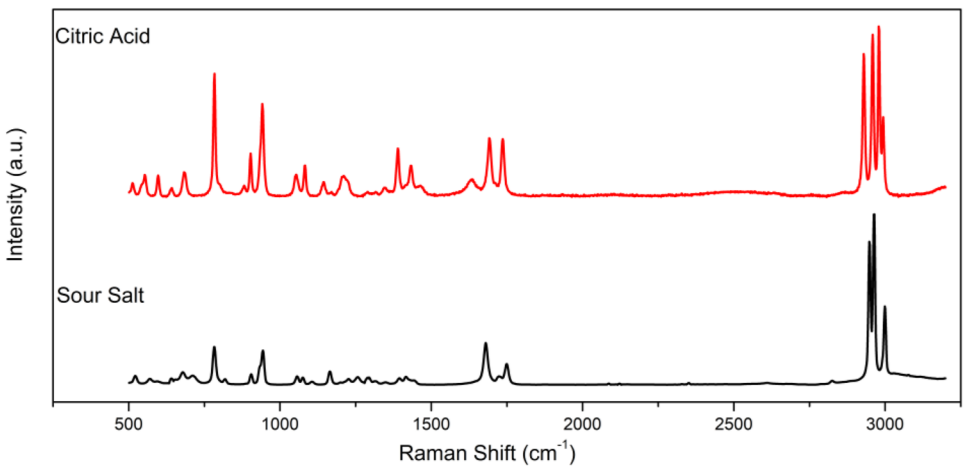


Fig. 2 Measured Raman spectra of sour salt and citric acid (color figure online)

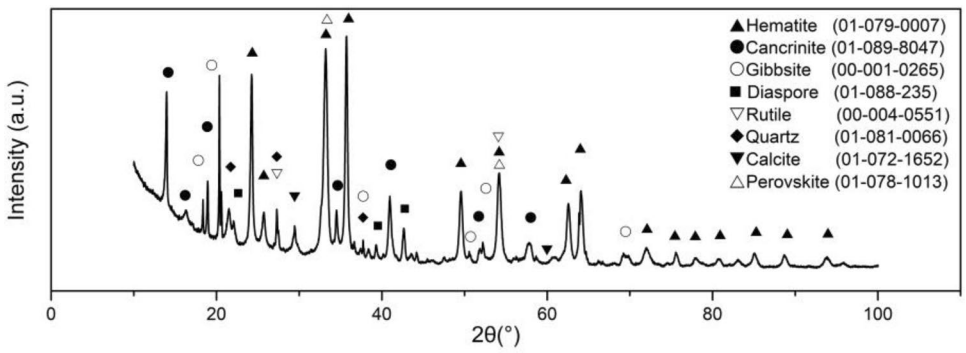


Fig. 3 XRD analysis of the red mud (*JCPDS numbers of compounds are given in the legend*)

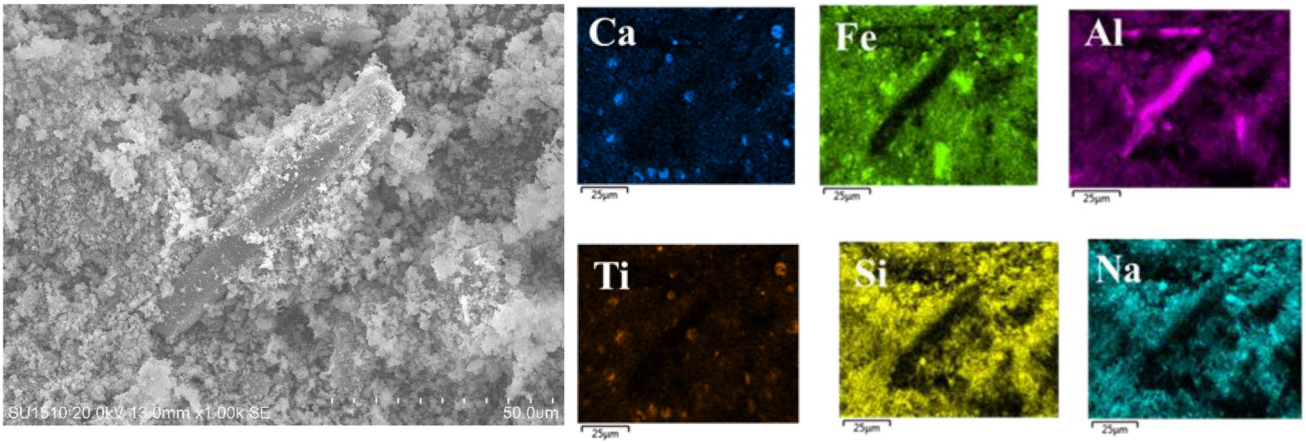


Fig. 4 SEM/EDX mapping of red mud sample (color figure online)

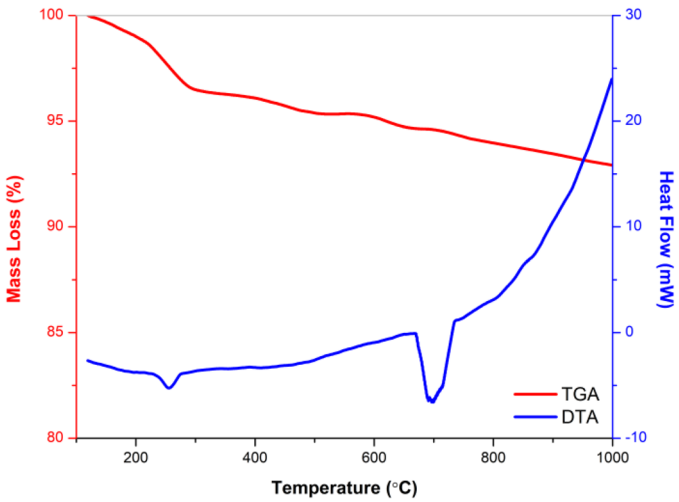


Fig. 5 Thermal analysis of red mud sample (color figure online)

($CaCO_3$) and rutile (TiO_2), but also as perovskite ($CaTiO_3$) which peaks are overlapped by those of hematite.

SEM/EDX analysis of the samples (Fig. 4) reveals that most of the particles have irregular shape; however, some geometric forms are visible. The EDX mapping shows that the geometric particles are exclusively aluminum based and are probably diaspore crystals [24]. On the other hand, the general dispersions of aluminum, silicone, and sodium are concomitant supporting the presence of feldspathoids. Similarly, with the lowest signal, calcium and titanium are distributed in the same regions supporting the presence of

perovskite. Finally, the iron is largely distributed with some specific particles.

The thermal behavior of the raw material was determined by using thermogravimetric (TG) and differential thermal analysis (DTA) between 25 and 1000 °C with 5 °C/min heating rate under nitrogen atmosphere (Fig. 5). At the end of the analysis, the total mass loss was 7% confirming the stability of the solid waste. However, three distinct steps are observed on the TG curve while only two marked peaks are present on the DTA curve. The loss at around 250 °C is associated with the removal of water from cancrinite [25] and the dehydroxylation of partial gibbsite involving the formation of boehmite phase (γ-AlO(OH)) [26] given by Eq. (2). The loss at about 450 °C is linked with the decomposition of this boehmite given by Eq. (3) [27–29]. The dehydroxylation of goethite [FeO(OH)] induced very weak mass loss (not visible on DTA curve) at around 350 °C given by Eq. (4) [30]. The endothermic peak seen on DTA curve at about 700 °C was attributed to the decomposition of calcite given by Eq. (5) and also associated with decarboxylation of cancrinite as a result of strong endothermic reaction [13, 25, 31]. The thermal behavior is compatible with the above characterization of the red mud. It suggests that the red mud not only consists of pure oxide, but it also contains hydroxides and different structures.

$$Al(OH)_3\ (s) \rightarrow AlO(OH)\ (s) + H_2O\ (g), \quad (2)$$

$$2\gamma\text{-}AlO(OH) \rightarrow \gamma\text{-}Al_2O_3 + H_2O\ (g), \quad (3)$$

$$2FeO(OH)\ (s) \rightarrow Fe_2O_3\ (s) + H_2O\ (g), \quad (4)$$

$$CaCO_3\ (s) \rightarrow CaO\ (s) + CO_2\ (g). \quad (5)$$

HCl Leaching

Since red mud is the residue obtained from the caustic treatment of the bauxite ore, it has a strong basic character. Therefore, highest interaction with the red mud is expected with HCl which completely dissociates in aqueous solution. As a result, depending on the acid concentration, the leaching time, and temperature, soluble and insoluble metal chlorides can be formed in the acidic media. The effect of the leaching parameters on the dissolution of Fe, Al, Ti, Si, Na and Ca has been investigated.

When processing has been realized at room temperature, most of the Fe, Ti, Al, and Ca present in the solid waste can be dissolved in the leaching solution (Fig. 6). Nevertheless, the highest dissolution rate specific to each metal has been obtained with 8 M acid concentration. With this concentration, whole Fe is dissolved after a 5-h treatment. For Ca as well as Al, the leaching efficiency with 4 M acid and 8 M acid are comparable after a 5-h process. This suggests that at room temperature, the maximum dissolution rate in HCl solution is about 75% for Ca and 80% for Al. Concerning Fe and Ti, the process has been just started after 5 h with 4 M acid while not observed with 1 M leaching solution. This implies that for initiating the process a minimum proton amount is required in solution. The hydronium ions are adsorbed onto the iron oxide surface lowering the iron–oxygen bonds, involving the separation of these nuclides [32]. Due to the high pH value (11.1 measured) of the red mud solution, 1 M acid is probably just enough for neutralization preventing the presence of free proton in the leaching solution.

Whatever the acid concentration, the dissolution of Na and Si ions is restricted (Fig. 6). After 1-h treatment, only about 6–7% of Na has been leached out. The highest rate obtained after the 5-h process does not exceed 9%, for each acid concentration the dissolution evolution can be considered as similar.

In the case of Si, the cation concentration has been decreased down to about 0% after 5-h treatment. The difference is based on the Si present in solution after 1-h process; 1% Si has been measured with the most concentrated acid (4 M and 8 M), while 10.7% Si has been dissolved within 1 M HCl. The leaching with 1 M solution leads to the gel formation which is attributed to the presence of silicon from sodium silicate (Na_4SiO_4), a byproduct of the Bayer process (6). The formation of Na_4SiO_4 is responsible of trapping Na atoms inside the gel structure.

$$SiO_2 + 4NaOH \rightarrow Na_4SiO_4 + 2H_2O. \quad (6)$$

In HCl medium, the presence of sodium silicate is due to the formation of silicic acid which polymerized via condensation to give the gel structure [Eqs. (7)–(8)].

$$Na_2SiO_3 + H_2O + 2HCl \rightarrow Si(OH)_4 + 2NaCl, \quad (7)$$

$$Si(OH)_4 + Si(OH)_4 \rightarrow (OH)_3Si{-}O{-}Si(OH)_3 + H_2O. \quad (8)$$

During the dissolution of silica-bearing minerals, silicic acid [$Si(OH)_4$] which is the monomer of the silica gel, is obtained from the hydrolysis of silica. The polymerization generates firstly oligomers, resulting then to the formation of a gel network. The gel consistency depends on the temperature, the acid concentration even the salts in the medium [33–35]. These parameters are directly affecting the silicon supersaturation index (SSI) which defines the maximum silicon solubility [36–38]. During the red mud leaching, the silicic acid originates from the cancrinite which involves the formation of sodium silicate. The highly acidic medium increases the coagulation of polymeric particles which accelerate the polymerization. These particles coalesced and fall down to the bottom of the leaching solution. On the other hand with 1 M HCl, the basic red mud solution is not acidified enough, therefore the electrostatic forces are more superior than the Van der Waals forces, as predicted

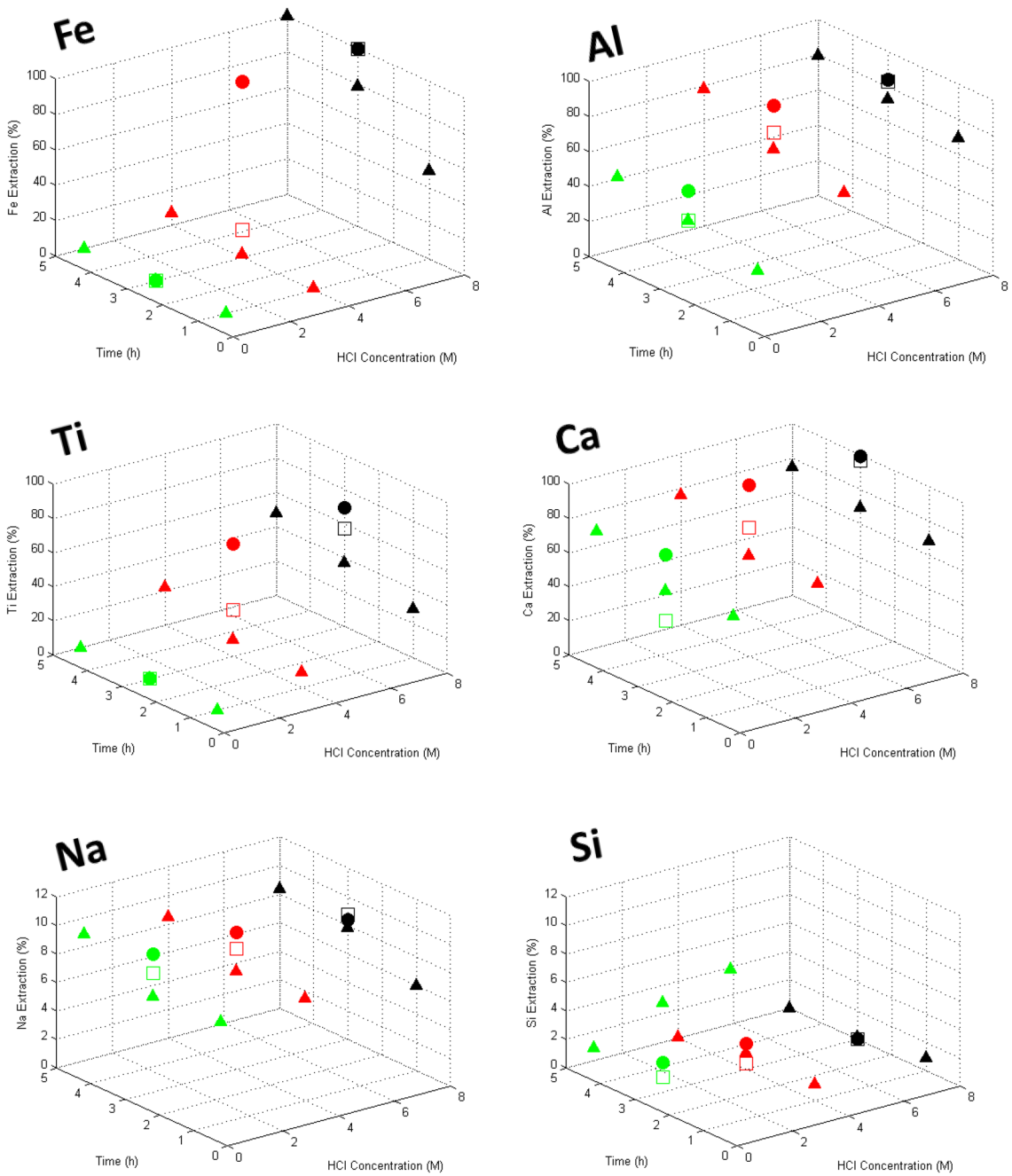


Fig. 6 Effects of HCl concentration (M), leaching time, and temperature on Fe, Al, Ti, Si, Na, Ca recovery rate in HCl solutions (300 rpm, 100 g/L pulp density). Green triangles: 1 M HCl, 25 °C, red triangles: 4 M HCl, 25 °C, black triangles: 8 M HCl, 25 °C, green squares: 1 M HCl, 50 °C, red squares: 4 M HCl, 50 °C, black squares: 8 M HCl, 50 °C, green circles: 1 M HCl, 100 °C, red circles: 4 M HCl, 100 °C, black circles: 8 M HCl, 100 °C (color figure online)

in the DLVO theory. In this situation, the flocculation of polymeric particles has been slowed down and controlled by the Brownian movement of the solvent molecule [39].

In spite of the dissolution of several cations within HCl solutions, 100% leaching rate has been only obtained for Fe with 8 M concentration. This suggests that cations are present under different forms with different reactivity. Table 2 shows that standard Gibbs free energy of compounds formation in red mud [40, 41]. Compounds within red mud can contain either one cation and oxygens/hydrogens or several cations and heteroatoms. Cation recovery from oxides and hydroxides implies the complete separation of elements, which means the counteracting of their Gibbs free energy which are below – 1000 kJ/mol. The two lowest energies

Table 2 Standard Gibbs free energy of compounds formation in red mud

Oxides	ΔG^0_{298} (kJ/mol)	Reference
Hematite	− 742	[41]
Gibbsite	− 1154	
Quartz	− 856	
Perovskite	− 1575	
Rutile	− 889	
Diaspore	− 922	
Calcite	− 1129	
Cancrinite	− 13,690	[40]

(− 489 and − 742 kJ/mol) concern the two Fe-based compounds, showing the effectiveness of 8 M HCl for their decomposition [Eq. (9)].

Compounds with several cations and heteroatoms (sodium titanate, calcite, and feldspathoids) have free energy above − 1000 kJ/mol, therefore their complete decomposition looks impossible. However, in acidic medium they can be partially decomposed into their simplest entities and/or ions. According to the XRD results, these compounds are the most present in red mud and they are at the origin of Ca, Ti, Al, and Na presence in the leaching medium.

Calcite and perovskite decompositions have induced the dissolutions of Ca and Ti [Reactions (10)–(11)], while Al is coming from feldspathoids [42, 43]. These aluminosilicates first yield aluminum hydroxide which also involves alumina ions at low pH values [Reactions (12)–(13)] [44, 45].

Finally, due to the Bayer process (caustic treatment) and the minerals (feldspathoids) present in red mud, high sodium concentration may be present in the leaching media, but only 6% of Na has been detected in solution. The sodium concentration has been conserved whatever the acid concentration, which means the leach solution contains the highest possible Na. It is assumed that sodium is present in two forms, firstly as $NaHCO_3$ which has at about 10% solubility in water [46] and secondly by the retention of some Na within the gel induced by the silicon.

$$FeO(OH) + 3H^+ \rightarrow Fe^{3+} + 2H_2O, \tag{9}$$

$$CaCO_3 + 2H^+ \rightarrow Ca^{2+} + CO_2 + H_2O, \tag{10}$$

$$CaTiO_3 + 2H^+ \rightarrow TiO_2 + Ca^{2+} + H_2O, \tag{11}$$

$$Na_8Al_6Si_6O_{24}(CO_3)(H_2O)_2 + 7H^+ + 16H_2O \rightarrow 8Na^+ + 6Al(OH)_3 + 6H_4SiO_4^- + HCO_3^-, \tag{12}$$

$$Al(OH)_3 + 3H^+ \rightarrow Al^{3+} + 3H_2O. \tag{13}$$

The leaching efficiency is sensitive to treatment temperature. 100 °C was the highest value chosen to evaluate the metal dissolution with different acid concentration during fixed 3 h (Fig. 6). Except Si and Na which behaviors have been described above, the highest efficiency values for Fe, Ca, Al, and Ti at 100 °C have been more or less obtained with 4 M acid. The recovery of whole Fe and Ca present in the red mud was due to the Gibbs free energy reduction of their respective compounds (Table 2). In fact, increasing the temperature is directly influencing the compounds entropy which affects the free energy according to Eq. (14) where G is the Gibbs free energy (kJ), H is the enthalpy, T is the temperature (K), S is the entropy (kJ/K) and Δ denotes the changing [Eq. (14)].

$$\Delta G = \Delta H - T \cdot \Delta S. \tag{14}$$

Concerning Al and Ti 100% leaching rate has not been reached, moreover the dissolution rate at 4 M is almost unchanged at 8 M. Therefore increasing the concentration is not influencing the leaching rate as observed at lower temperatures. This situation involves that these metals are present in red mud within two different compounds at least.

The process temperature is not influencing the overall behavior of Si which has been dissolved by a few percent within HCl solution. Moreover, increasing the acid concentration leads to the lowest dissolution, suggesting that the polymerization rate has been increased.

Finally, the all of the Na in the red mud cannot be extracted even at 100 °C and 8 M HCl. But the dissolution rate tends to increase when the temperature increases. However, at 8 M and 100 °C less Na is extracted than at 4 M and 100 °C. This behavior is similar to Si, suggesting that the formation of silica gel at the highest HCl concentration acts as a trap for Na atoms.

Citric Acid Leaching

For the preparation with 10, 30, and 50 g solid, before adding red mud sample, the concentrations selected in respect of the weak triprotic citric acid solution are 1.04, 3.13, and 5.21 M, respectively. The acid concentration as well as the first pKa helps to adjust the pH of organic polyacid solution. Corresponding to the masses of added acid, the measured pH for these solutions were 1.82, 1.31, and 0.8, respectively. Thus, the pH of the highest concentrated citric acid solution is close to the one of the lowest concentrated hydrochloric acid solution (1 M). That is the reason why Fe and Ti, which are dissolved at room temperature with 4 M HCl solution, are not detected within the citric acid solutions even at 5.21 M concentration. However, the acidity is enough to induce the formation of Si-based gel, also observed with HCl solution. In both acidic solutions, except the value of the highest dissolved fraction, the leaching behavior of Si is comparable. The amount of dissolved Si first increases to a

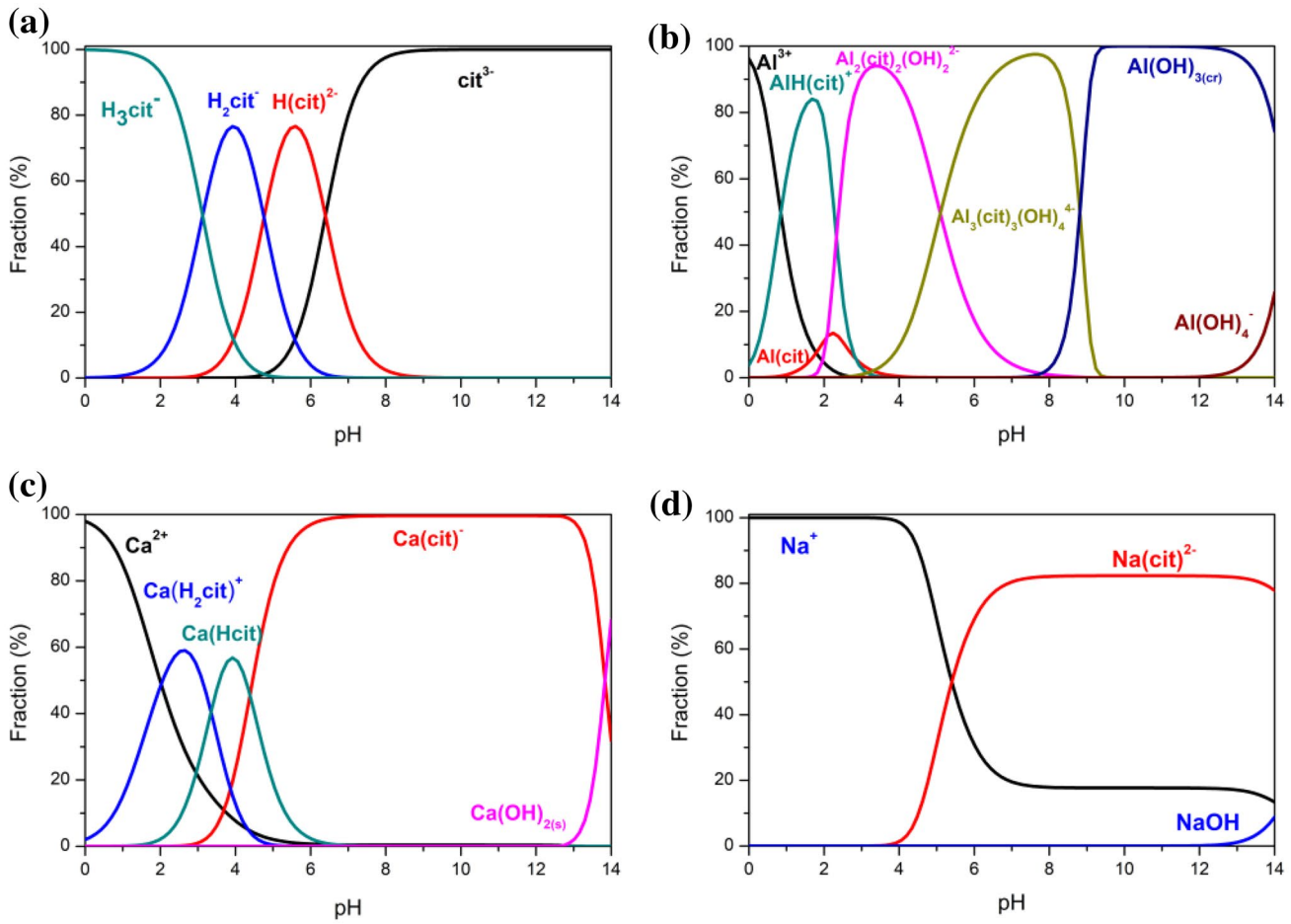


Fig. 7 Theoretical formation of citrate species with 1 M citric acid solution (**a**) and the formation of metal species in the presence of 1 M cation (**b** Al^{3+}, **c** Ca^{2+}, **d** Na^{+}) within 1 M citric acid solution (*Medusa software*, *Royal Institute of Technology*, *Sweden*) (color figure online)

certain maximum value, after which it decreases over time according to the mechanism described above.

The concentration profiles for the elements within citric acid for Al, Ca, and Na are similar to those within HCl solution. After 1-h treatment, at each acid concentration, a maximum dissolution is obtained, which then changes according to the acidic concentration. Compared with hydrochloric acid under the same conditions, the highest leached-out metal amount is comparable for Na, while it is slightly lower for Ca. This suggests that the decomposition of calcite and sodium titanate is possible within citric acid. Finally, unlike with HCl medium, the dissolution of Al decreases with the increasing acidic concentration. It is probably due to an additional effect related to the organic acid during the decomposition of feldspathoids.

The citric acid contains three different carboxylic acid groups with three different pKa values: this means that hydroniums are released step by step in solution [Eqs. (15)–(17)]. Therefore, according to the pH values, three different organic anions can be present in aqueous solution.

$$H_3Cit \rightleftharpoons H^+ + H_2Cit^-, \quad (15)$$

$$H_2Cit^- \rightleftharpoons H^+ + HCit^{2-}, \quad (16)$$

$$HCit^{2-} \rightleftharpoons H^+ + Cit^{3-}. \quad (17)$$

Anions from citric acids can react with metallic cations present in solution to possibly form complexes. Depending on the leaching solution's pH, the complex charge changes until it reaches electroneutrality. This assumes the formation of solid salts like CaHCit, AlCit, or NaH_2Cit. Several parameters can influence the solution's composition like the concentration, the temperature, and the specificity of the present ions (Debye–Hückel Theory).

In the present situation, the properties and the concentrations of ions coming from the citric acid are well known, but those from red mud are uncontrollable. Therefore, an analytic study of the media is not feasible. However, by means of a theoretical approach, indications concerning the metal species' behavior in solutions can be understood. Supposing that the medium only contains Al, Ca, or Na at 1 mol, the

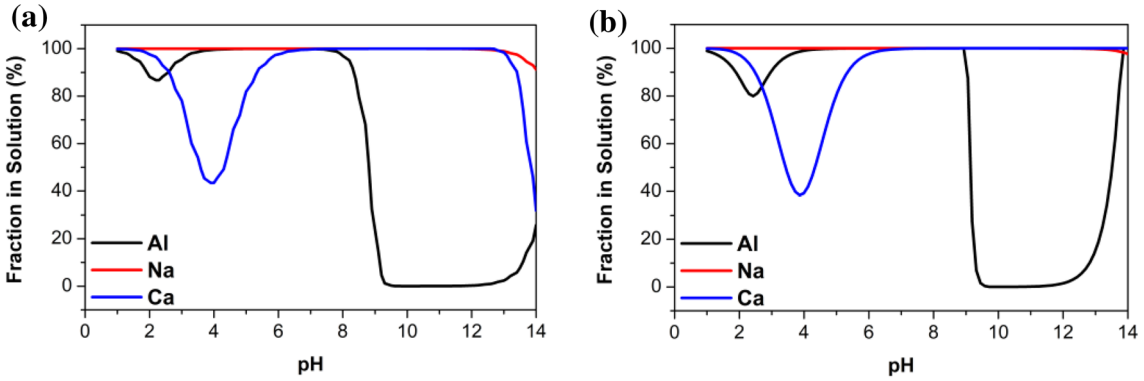


Fig. 8 Theoretical dissolution of 1 M metal (Al^{3+}, Ca^{2+}, or Na^{+}) within 1 M citric acid solution (**a**), Theoretical dissolution of metal species within 1 M citric acid solution containing a mix of 0.020 M Ca^{2+}, 0.168 M Al^{3+}, and 0.023 M Na^{+} (**b**) (*Medusa software*, *Royal Institute of Technology*, *Sweden*) (color figure online)

theoretical dissolution curve within 1 M citric acid has been drawn (Fig. 7).

Theoretically, citric acid starts to release its first hydronium at pH 2, then the higher concentrations of the anions are observed at pH 4, at pH 6, and at pH above 8. The formation of different metal species with the increasing pH is then predicted for Al and Ca complexes. The electroneutral AlCit and CaHCit species are obtained between pH 0–4 and pH 2–6, respectively. Concerning the Na species, above pH 4, the fraction of free cations decreases in profit to the formation of $NaCit_2^-$ complex; no precipitation is waited below pH 12. Considering that only charged species are dissolved, a fraction of metal species within 1 M aqueous citric acid solution has been predicted (Fig. 8a). Thus, the concentration of Al should partially decrease when pH value is between 1 and 4 and totally decrease with pH above 8. In the same manner, the concentration of Ca should partially decrease with pH values between 2 and 6 and totally decrease with pH above 13. Regarding Na, its precipitation just starts at pH 13.

In order to simulate the real solution, based on the XRF results, it has been determined that the weight percents of Al, Na, and Ca in red mud are 10.8%, 7.70%, and 1%, respectively. Supposing that the highest extraction rates are obtained with hydrochloric acid leaching, the highest possible Al^{3+}, Na^{+}, and Ca^{2+} concentrations within citric acid are estimated to be 0.168 M, 0.023 M, and 0.020 M. Since the lowest concentrated citric acid solution is 1.04 M, citrate-based anions are always in excess within the medium. Taking into account these values, the theoretical dissolution of metal species within 1.04 M leaching solution at different pH values has been estimated (Fig. 8b). The precipitation behavior of cations has been slightly modified. The solid fractions of Al at pH between 1 and 4 and Ca at pH between 2 and 6 show slight increase. The total precipitation of Al becomes possible only between pH 9 and 12. Finally, at pH 14, no precipitation of metal hydroxides can be observed.

The theoretical approach shows that precipitation of metal salts is responsible for the decrease of Al- and Ca-based species with the increasing concentration of citric acid, similar to the previous works [47, 48]. Regarding Na, its precipitation should be possible only at pH above 13 which is higher than the one of the red mud solution. Nevertheless, as seen previously with HCl leaching, in the presence of silicon-based gel, Na^{+} ions can be retained within the gel structure. Same mechanism can be possible herein, but with pH below 8, Na^{+} is the major species, while with pH above 8, $NaCit_2^-$ is mainly present. This suggests that sodium retention within silicon-based gel is better when the species in solution are free cations.

Finally, the metal fraction in solution is continuously changing with time and with acid concentration, especially at 3.13 M and 5.21 M. This is the evidence that kinetic parameters influence the metal leaching with citric acid.

Dissolution rates at different temperatures (25 °C, 50 °C, and 100 °C) and different citric acid concentrations over a duration of 3 h show that the dissolution behavior is evolving (Fig. 9). Increasing the temperature of the media improves the leaching rate; however, the results at 50 °C are slightly better than those at 100 °C. At the former temperature, decomposition of citric acid is more marked, and its efficiency for leaching starts to decrease [17, 49]. This trend is not visible for Ti, where dissolution rate is started and then increased with the increasing temperature (up to 7% at 100 °C), hiding then the thermal decomposition of citric acid. Concerning the other elements; Si dissolution is still very weak and the gel formation is kept, while Al, Ca, and Na have once again a common similar behavior. The difference is that the dissolved metal amount is reduced with

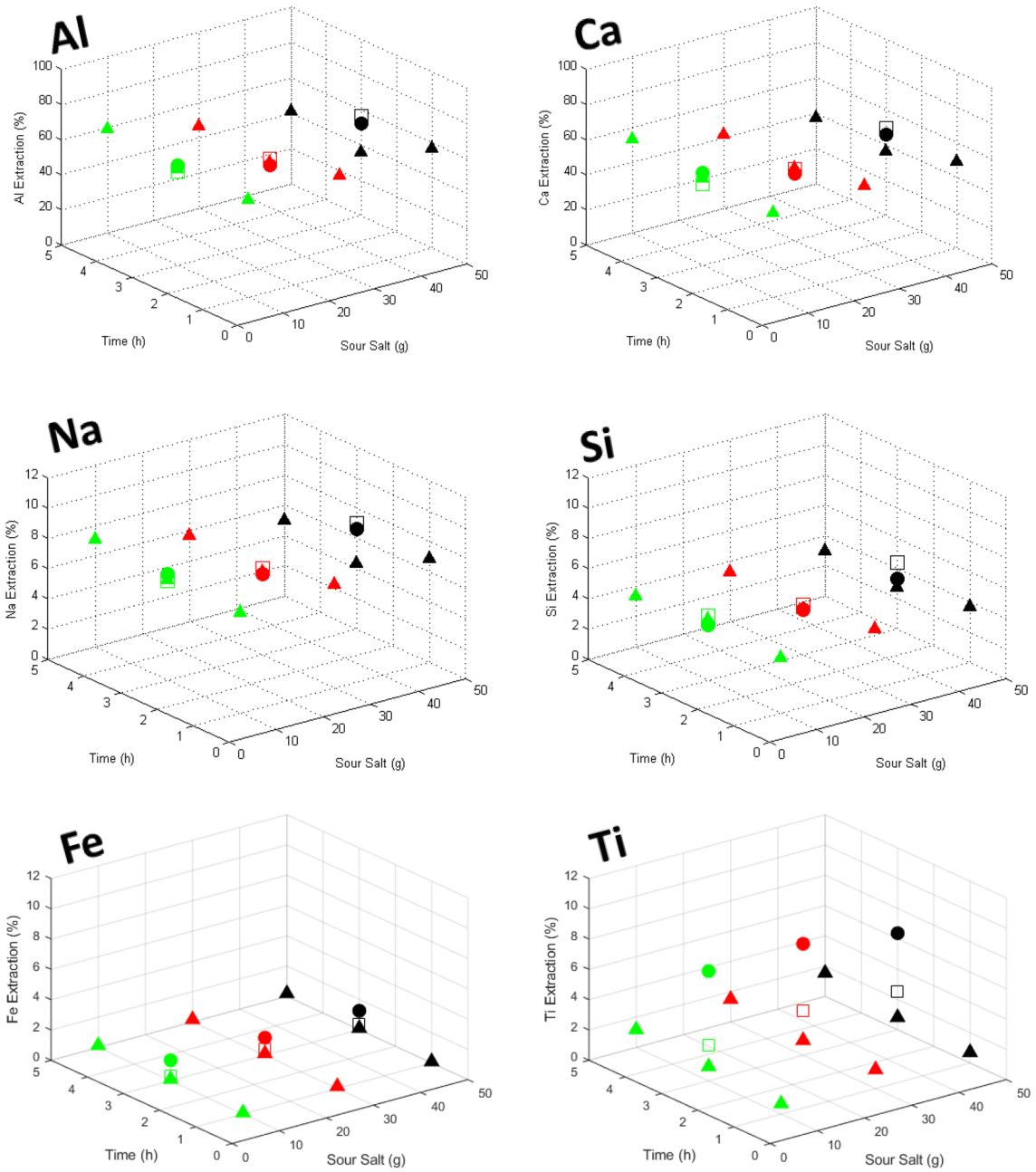


Fig. 9 Effects of citric acid concentration, leaching time, and temperature on the extractions of Fe, Al, Ti, Si, Na, and Ca in citric acid solutions. Green triangles: 10 g SS, 25 °C, red triangles: 30 g SS, 25 °C, black triangles: 50 g SS, 25 °C, green squares: 10 g SS, 50 °C, red squares: 30 g SS, 50 °C, black squares: 50 g SS, 50 °C, green circles: 10 g SS, 100 °C, red circles: 30 g SS, 100 °C, black circles: 50 g SS, 100 °C (color figure online)

3.13 M citric acid, but the leached out metals are increased with 5.21 M citric acid. This evolution shows that the complex formation is completed, and the dissociation rate of citric acid is accelerated with high acid concentration and temperature. On the other hand, Fe leaching is started with difficulty at 100 °C, but the dissolution rate does not trespass 1.5%.

Leaching Residues

Spectroscopic analysis has demonstrated that the treatment with 8 M HCl at 100 °C for 3 h is enough to reach stabilized leaching media with maximum metal dissolution under these conditions. Thus, insoluble elements present within leaching residues have been characterized via EDX mapping

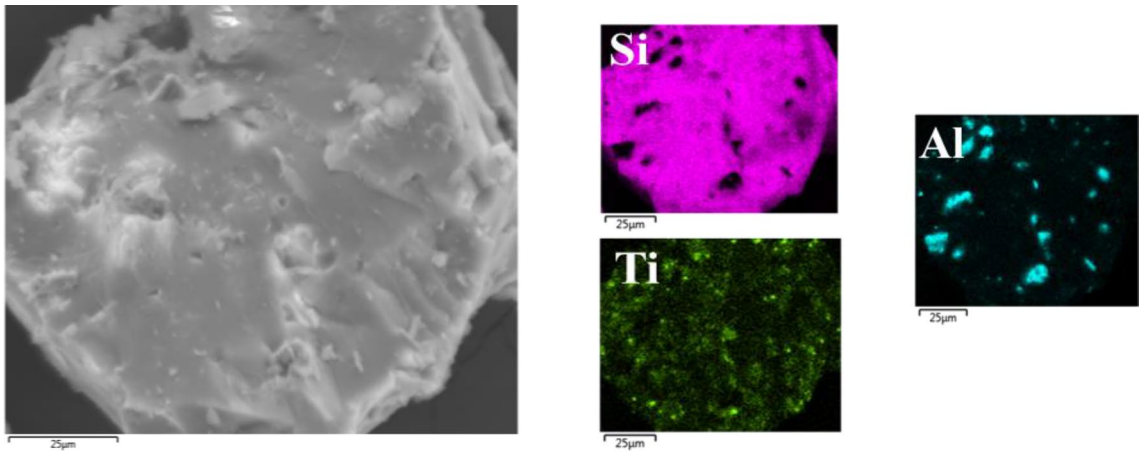


Fig. 10 SEM/EDX mapping of 8 M HCl leaching residue (*T* 100 °C, 3 h, 300 rpm, 100 g/L pulp density) (color figure online)

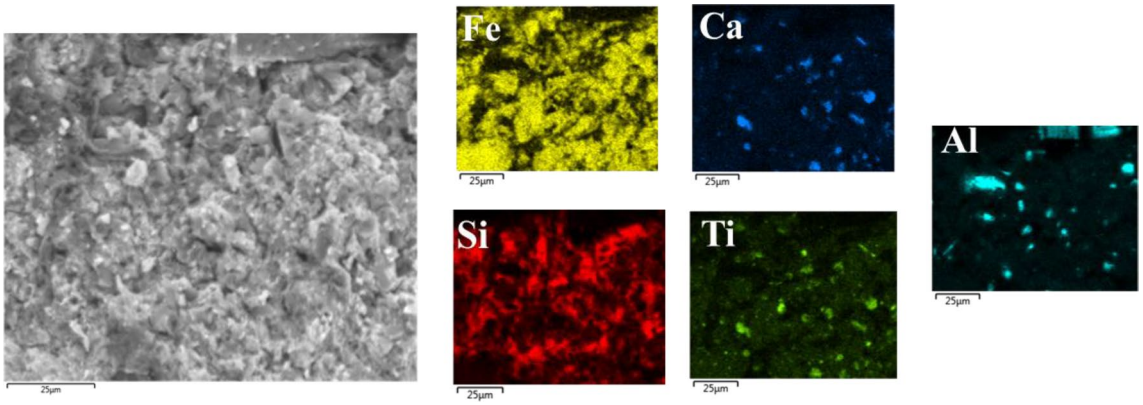


Fig. 11 SEM/EDX mapping of 50 g citric acid leaching residue (*T* 100 °C, 3 h, 300 rpm, 100 g/L pulp density) (color figure online)

(Fig. 10). No traces of Fe, Ca, and Na have been detected confirming the complete dissolution of these metals during the process. Si, Al, and Ti are present within the final solid sample. Especially, the presence of Si is strongly marked throughout the whole sample except in the presence of Al. In other worlds, Al- and Si-based compounds are well separated in the residue. Even if the Al-rich regions are lower, the contrast is less marked with Ti-based compounds which are finely dispersed with some highly concentrated regions.

The SEM–EDX analysis of the leaching residue obtained by processing at 100 °C and with 5.21 M citric acid solution reveals the omnipresence of Fe and Si, which means that these metals are not dissolved (Fig. 11). Concerning Al-rich region, the presence of regular- and irregular-shaped particles suggests that Al is under different forms. Similarly, Ti is present either as isolated particles or more largely together with Ca. Whole observations are in accordance with ICP analysis and support the suggested dissolution mechanisms.

Leaching residues (Figs. 10, 11) have also been analyzed by the XRD method to determine undissolved phases after high acidic leaching process (100 °C). The XRD patterns of leaching residues and red mud are depicted in Fig. 12. It shows that hematite, cancrinite, and calcite in red mud have been dissolved completely with 8 M HCl at 100 °C. Moreover, XRD results also confirm that the amorphous and crystalline silicon phases are retained in the HCl leaching residue as seen in Fig. 10. Although hematite and perovskite have been completely dissolved, rutile has been detected in the HCl leaching residue. This implies that the rutile phase in the red mud is more stable than hematite as mentioned in the literature [10] in accordance with the above thermodynamic data (Table 2).

Hematite is detected in the XRD pattern of the citric acid leaching residue, showing that just cancrinite and calcite are dissolved. It suggests that aluminum and calcium ions have been transformed into leaching solution from cancrinite and calcite minerals in red mud.

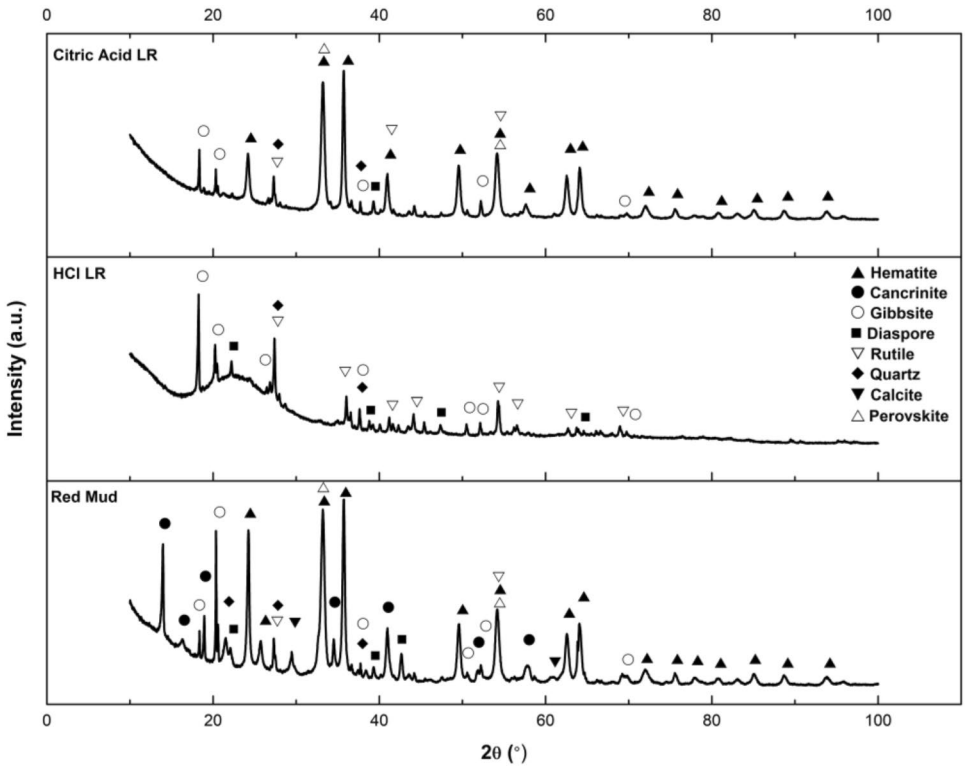


Fig. 12 XRD patterns of leaching residues and red mud (*LR* leaching residue)

Table 3 Kinetic constants and coefficients of determination for Fe, Al, and Ti dissolutions with concentrated HCl (*T* 25 °C)

HCl concentration	Elements	Fe	Al	Ti
4 M	R^2	0.893	0.9264	0.8968
	k	2×10^{-4} min^{-1}	272×10^{-4} mol/L/min	7×10^{-4} min^{-1}

Kinetic Approaches

The dissolution of cations within red mud has changed over time and temperature to sometimes reach an upper limit. This suggests the leaching rates are influenced by kinetic parameters [50], but the timeframe of measurements is inadequate for a complete kinetic study. First of all, only data concerning Fe, Al, and Ti obtained with 4 M HCl have been considered. In fact, possibly the whole cation dissolution is observed before 5 h with 8 M acid, which prevents tracking the leaching rate with time. Second, by using the first- and second-order kinetic equations (1) and (2), the order of the leaching reactions has been estimated by considering the coefficient of determination (R^2) (Table 3). Finally, activation energies of the reactions were calculated thanks to the Arrhenius law (3).

(1) First order: $\ln [A] = \ln [A]_0 - kt$ (k unit/min),
(2) second order: $1/[A] = 1/[A]_0 - kt$ (k unit mol/L/min),
(3) $k = \exp(E_a/kT) \Rightarrow E_a = R{\cdot}T{\cdot}\ln k$ ($R = 8.314$ J/K/mol).

By comparing all the R^2 value, the leaching of Fe and Ti are more suitable to a first-order reaction, while the dissolution of Al corresponds more to a second-order reaction. Regarding the literature, the first order has been referred for Fe dissolved from hematite [51]; however, no studies mentioned kinetic orders for Al dissolved from cancrinite and Ti dissolved from perovskite.

The calculated kinetic constant k for all dissolutions showed that the leaching rate of Al is several times higher than those of Fe and Ti. The kinetic constants followed an Arrhenius law depending on the temperature, and therefore, the activation energies for all dissolutions have been calculated. The value of the activation energy corresponds to the slope of the graph $\ln k = f(1/T)$ (Fig. 13).

The calculated activation energy for the iron recovery with 4 M HCl is 52.5 kJ/mol. This value is close to the activation energy of 54.83 kJ/mol obtained for the leaching of the coal mining waste [52]. In the literature, highest values are also reported as 62–79 kJ/mol [53] and 81 kJ/mol [51], but both results are obtained directly during the leaching of bauxite ores. In other words, the pretreatments of the metal

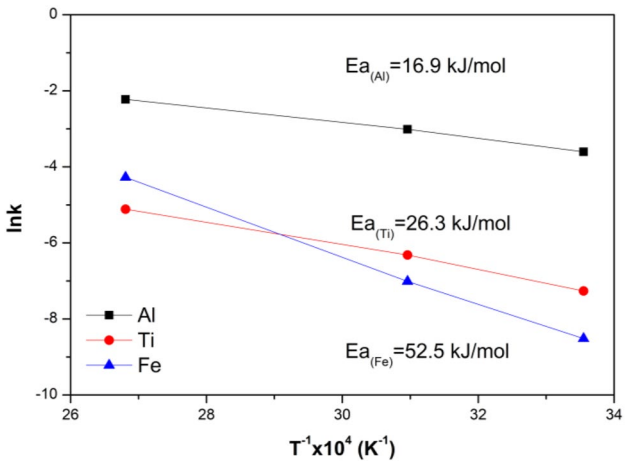


Fig. 13 Evolution of the dissolution kinetic constant with 4 M HCl at 25, 50, and 100 °C (color figure online)

sources, like grain size reduction and other thermal or thermochemical processes, influence the reactivity.

Concerning the titanium recovery, the calculated activation energy is about 26.3 kJ/mol, while for the aluminum recovery it is about 16.9 kJ/mol. For both metals, two separate sources are present in red mud: perovskite and rutile for Ti, and gibbsite and cancrinite for Al. Referring to the XRD results, after leaching, rutile and gibbsite are present, and therefore, it can be considered that the calculated activation energies correspond to the recovery of Ti from perovskite and Al from cancrinite.

Conclusions

Red mud is the residue of the Bayer process which consists of oxide structures with different reactivities. When using strong hydrochloric acid and weak citric acid at different concentrations and temperatures, selective recovery of the most present metals are observed.

The leaching temperature is the most efficient parameter with strong acid, and by coupling it with enough acid concentration, the metal dissolution is started. Thus, all the Fe and Ca, more than 60% of Ti, and 80% of Al can be dissolved with 4 M HCl at 100 °C. However, a duration of only a few hours is required to complete the leaching process, which means that kinetic parameters govern the metal leaching within the strong acid. The activation energies found for Fe, Al, and Ti dissolutions are found to conform to those in the literature. Finally, whole metals have not been dissolved due to the presence of different cation sources which are not activated even at 100 °C with 8 M HCl.

Within organic acid, the metal leaching is more dependent on the complex formation that can lead to the formation of solids in function of the pH. The dissolved metals amount is lower than the one with HCl reaching 50% for Ca and 60% for Al. These values are obtained at low concentrations, and they do not really change with the increasing temperature or the concentration.

This study shows that the dissolution of cations present in metal are dependent not only on the leaching solutions and process conditions, but also on the cation-rich minerals. Regarding the mineral reactivity and the acid properties, selective cation dissolutions are possible, which can involve Ca- and Al-rich solutions and Fe- and Ti-rich solutions. Hydrometallurgical processes can be used to recover cations separately. Finally, the solid residue at the end of the process is rich in oxides like SiO_2, TiO_2, or Al_2O_3 which can be directly used in the ceramic industry, for example.

Acknowledgements The authors thank Eti Alüminyum A.Ş. administration and its General Director Mehmet Arkan for all the support by providing the red mud samples; and Assoc. Prof. Mehmet Muzaffer Karadağ for his valuable advice and support; and BITAM Central Laboratory of Necmettin Erbakan University and the Analysis Laboratory of Aciöz Rafinasyon ve Rejenerasyon for the help in the sample analysis.

Compliance with Ethical Standards

Conflicts of interest The authors declare no conflicts of interest.

References

1. Borra CR, Blanpain B, Pontikes Y, Binnemans K, Van Gerven T (2016) Smelting of bauxite residue (red mud) in view of ıron and selective rare earths recovery. J Sustain Metall 2:28–37. https://doi.org/10.1007/s40831-015-0026-4
2. Mishra B, Gostu S (2015) Opportunities for high volume commercial products conversion from bauxite residue. İn: Bauxite residue valorisation and best practices conference (Leuven, Belgium, 5–7 October 2019)
3. Abhilash SS, Meshram P, Pandey BD, Behera PK, Satpathy BK (2014) Red Mud: a secondary resource for rare earth elements. In: International bauxite, alumina and aluminium symposium. The IBAAS Binder, pp 148–162
4. Agatzini-Leonardou S, Oustadakis P, Tsakiridis PE, Markopoulos C (2008) Titanium leaching from red mud by diluted sulfuric acid at atmospheric pressure. J Hazard Mater 157:579–586. https://doi.org/10.1016/j.jhazmat.2008.01.054
5. Balomenos E, Panias D, Pontikes Y (2015) MUD2METAL: a holistic flow sheet for the Bauxite Residue valorisation. In: Bauxite residue valorisation and best practices conference, Leuven, 5–7 October, pp 129–136
6. Liu Y, Naidu R (2014) Hidden values in bauxite residue (red mud): recovery of metals. Waste Manag 34:2662–2673. https://doi.org/10.1016/j.wasman.2014.09.003
7. Mishra B, Gostu S (2017) Materials sustainability for environment: red-mud treatment. Front Chem Sci Eng 11:483–496. https://doi.org/10.1007/s11705-017-1653-z
8. Borra CR, Mermans J, Blanpain B, Pontikes Y, Binnemans K, Van Gerven T (2016) Selective recovery of rare earths from bauxite

residue by combination of sulfation, roasting and leaching. Miner Eng 92:151–159. https://doi.org/10.1016/J.MINENG.2016.03.002
9. Borra CR, Blanpain B, Pontikes Y, Binnemans K, Van Gerven T (2017) Recovery of rare earths and major metals from bauxite residue (red mud) by alkali roasting, smelting, and leaching. J Sustain Metall 3:393–404. https://doi.org/10.1007/s40831-016-0103-3
10. Pepper RA, Couperthwaite SJ, Millar GJ (2016) Comprehensive examination of acid leaching behaviour of mineral phases from red mud: recovery of Fe, Al, Ti, and Si. Miner Eng 99:8–18. https://doi.org/10.1016/j.mineng.2016.09.012
11. Xue S, Zhu F, Kong X, Wu C, Huang L, Huang N, Hartley W (2016) A review of the characterization and revegetation of bauxite residues (red mud). Environ Sci Pollut Res 23:1120–1132. https://doi.org/10.1007/s11356-015-4558-8
12. Crowson P (1996) Aluminium/bauxite/alumina. In: Minerals handbook 1996–97. Palgrave Macmillan UK, London, pp 1–18. https://doi.org/10.1007/978-1-349-13793-0_1
13. Borra CR, Pontikes Y, Binnemans K, Van Gerven T (2015) Leaching of rare earths from bauxite residue (red mud). Miner Eng 76:20–27. https://doi.org/10.1016/J.MINENG.2015.01.005
14. Astuti W, Hirajima T, Sasaki K, Okibe N (2016) Comparison of effectiveness of citric acid and other acids in leaching of low-grade Indonesian saprolitic ores. Miner Eng 85:1–16. https://doi.org/10.1016/j.mineng.2015.10.001
15. Astuti W, Hirajima T, Sasaki K, Okibe N (2016) Comparison of atmospheric citric acid leaching kinetics of nickel from different Indonesian saprolitic ores. Hydrometallurgy 161:138–151. https://doi.org/10.1016/j.hydromet.2015.12.015
16. Demir F, Dönmez B (2008) Optimization of the dissolution of magnesite in citric acid solutions. Int J Miner Process 87:60–64. https://doi.org/10.1016/j.minpro.2008.01.006
17. Gharabaghi M, Irannajad M, Noaparast M (2010) A review of the beneficiation of calcareous phosphate ores using organic acid leaching. Hydrometallurgy 103:96–107. https://doi.org/10.1016/j.hydromet.2010.03.002
18. Irannajaad M, Meshkini M, Azadmehr AR (2013) Leaching of zinc from low grade oxide ore using organic acid. Physicochem Probl Miner Process 49:547–555. https://doi.org/10.5277/ppmp130215
19. Shabani MA, Irannajad M, Azadmehr AR (2012) Investigation on leaching of malachite by citric acid. Int J Miner Metall Mater 19:782–786. https://doi.org/10.1007/s12613-012-0628-9
20. Lide DR (2003) Handbook of chemistry and physics. CRC Press, Boca Raton
21. McDonald RG, Whittington BI (2008) Atmospheric acid leaching of nickel laterites review. Part II. Chloride and bio-technologies. Hydrometallurgy 91:56–69. https://doi.org/10.1016/j.hydromet.2007.11.010
22. Zhu X, Li W, Guan X (2015) Kinetics of titanium leaching with citric acid in sulfuric acid from red mud. Trans Nonferr Met Soc China 25:3139–3145. https://doi.org/10.1016/S1003-6326(15)63944-9
23. Huang Z, Chen X, Li Y, Chen J, Lin J, Wang J, Lei J, Chen R (2013) Quantitative determination of citric acid in seminal plasma by using Raman spectroscopy. Appl Spectrosc 67:757–760. https://doi.org/10.1366/12-06902
24. Wang X, Dai S, Ren D, Yang J (2011) Mineralogy and geochemistry of Al-hydroxide/oxyhydroxide mineral-bearing coals of Late Paleozoic age from the Weibei Coalfield, Southeastern Ordos Basin, North China. Appl Geochem 26:1086–1096. https://doi.org/10.1016/j.apgeochem.2011.03.013
25. Hassan I (1996) The thermal behavior of cancrinite. Can Mineral 34:893–900
26. Redaoui D, Sahnoune F, Heraiz M, Raghdi A (2017) Mechanism and kinetic parameters of the thermal decomposition of gibbsite $Al(OH)_3$ by thermogravimetric analysis. Acta Phys Pol A 131:562–565
27. Atasoy A (2007) The comparison of the Bayer process wastes on the base of chemical and physical properties. J Therm Anal Calorim 90:153–158. https://doi.org/10.1007/s10973-005-7671-y
28. Callister WD, Cutler IB, Gordon RS (1966) Thermal decomposition kinetics of boehmite. J Am Ceram Soc 49:419–422. https://doi.org/10.1111/j.1151-2916.1966.tb15408.x
29. Pascual J, Corpas FA, López-Beceiro J, Benítez-Guerrero M, Artiaga R (2009) Thermal characterization of a Spanish red mud. J Therm Anal Calorim 96:407–412. https://doi.org/10.1007/s10973-008-9230-9
30. Atasoy A (2005) An investigation on characterization and thermal analysis of the Aughinish red mud. J Therm Anal Calorim 81:357–361. https://doi.org/10.1007/s10973-005-0792-5
31. Atasoy A (2011) Reduction of ferric oxides ın the red mud by the aluminıothermic process. İn: 6th International advanced technologies symposium, Elazig, Turkey, pp 16–18
32. Cornell RM, Schwertmann U (2003) The iron oxides: structure, properties, reactions, occurrences and uses. Wiley, Weinheim
33. Alkan G, Yagmurlu B, Cakmakoglu S, Hertel T, Kaya Ş, Gronen L, Stopic S, Friedrich B (2018) Novel approach for enhanced scandium and titanium leaching efficiency from bauxite residue with suppressed silica gel. Sci Rep 8:5676. https://doi.org/10.1038/s41598-018-24077-9
34. Rivera RM, Ulanaers B, Ounoughene G, Binnemans K, Gerven TV (2017) Behaviour of silica during metal recovery from bauxite residue by acidic leaching. In: Travaux 46, proceedings of 35th ınternational ICSOBA conference, Hamburg, Germany, 2–5 October 2017
35. Tanaka M, Takahashi K (2007) Study on the salting-out effect using silica species by FAB-MS. J Solut Chem 36:27–37. https://doi.org/10.1007/s10953-006-9101-6
36. Kokhanenko P, Brown K, Jermy M (2016) Silica aquasols of incipient instability: synthesis, growth kinetics and long term stability. Colloids Surf A 493:18–31. https://doi.org/10.1016/j.colsurfa.2015.10.026
37. Voßenkaul D, Birich A, Müller N, Stoltz N, Friedrich B (2016) Hydrometallurgical processing of eudialyte bearing concentrates to recover rare earth elements via low-temperature dry digestion to prevent the silica gel formation. J Sustain Metall 3:79–89. https://doi.org/10.1007/s40831-016-0084-2
38. Iler RK (1979) The chemistry of silica: solubility, polymerization, colloid and surface properties, and biochemistry. Wiley, New York
39. Gorrepati EA, Wongthahan P, Raha S, Fogler HS (2010) Silica precipitation in acidic solutions: mechanism, pH effect, and salt effect. Langmuir 26:10467–10474. https://doi.org/10.1021/la904685x
40. Kurdakova SV, Grishchenko RO, Druzhinina AI, Ogorodova LP (2014) Thermodynamic properties of synthetic calcium-free carbonate cancrinite. Phys Chem Miner 41:75–83. https://doi.org/10.1007/s00269-013-0625-1
41. Robie RA, Hemingway BS, Fisher JR (1978) Thermodynamic properties of minerals and related substances at 298.15 K and 1 bar (105 Pascals) pressure and at higher temperatures. Bulletin 2131. https://doi.org/10.3133/b2131
42. Nesbitt HW, Bancroft GM, Fyfe WS, Karkhanis SN, Nishijima A, Shin S (1981) Thermodynamic stability and kinetics of perovskite dissolution. Nature 289:358–362. https://doi.org/10.1038/289358a0
43. Wang Y, Qi T, Chu J, Zhao W (2010) Production of TiO_2 from $CaTiO_3$ by alkaline roasting method. Rare Met 29:162–167. https://doi.org/10.1007/s12598-010-0028-0
44. Kong X, Li M, Xue S, Hartley W, Chen C, Wu C, Li X, Li Y (2017) Acid transformation of bauxite residue: conversion of its

alkaline characteristics. J Hazard Mater 324:382–390. https://doi.org/10.1016/j.jhazmat.2016.10.073
45. Palmer DA, Wesolowski DJ (1992) Aluminum speciation and equilibria in aqueous solution: II. The solubility of gibbsite in acidic sodium chloride solutions from 30 to 70 °C. Geochim Cosmochim Acta 56:1093–1111. https://doi.org/10.1016/0016-7037(92)90048-N
46. Kim S, Thiessen PA, Bolton EE, Chen J, Fu G, Gindulyte A, Han L, He J, He S, Shoemaker BA, Wang J, Yu B, Zhang J, Bryant SH (2016) PubChem substance and compound databases. Nucleic Acids Res 44:D1202–D1213. https://doi.org/10.1093/nar/gkv951
47. Danks AE, Hall SR, Schnepp Z (2016) The evolution of 'sol–gel' chemistry as a technique for materials synthesis. Mater Horiz 3:91–112. https://doi.org/10.1039/C5MH00260E
48. Li L, Ge J, Wu F, Chen R, Chen S, Wu B (2010) Recovery of cobalt and lithium from spent lithium ion batteries using organic citric acid as leachant. J Hazard Mater 176:288–293. https://doi.org/10.1016/j.jhazmat.2009.11.026
49. Habbache N, Alane N, Djerad S, Tifouti L (2009) Leaching of copper oxide with different acid solutions. Chem Eng J 152:503–508. https://doi.org/10.1016/j.cej.2009.05.020
50. Crundwell FK (2014) The mechanism of dissolution of minerals in acidic and alkaline solutions: Part I—a new theory of non-oxidation dissolution. Hydrometallurgy 149:252–264. https://doi.org/10.1016/j.hydromet.2014.06.009
51. Reddy B, Mishra S, Banerjee G (1999) Kinetics of leaching of a gibbsitic bauxite with hydrochloric acid. Hydrometallurgy 51:131–138. https://doi.org/10.1016/S0304-386X(98)00075-9
52. Cui L, Guo Y, Wang X, Du Z, Cheng F (2015) Dissolution kinetics of aluminum and iron from coal mining waste by hydrochloric acid. Chin J Chem Eng 23:590–596. https://doi.org/10.1016/j.cjche.2014.05.017
53. Paspaliaris Y, Tsolakis Y (1987) Reaction kinetics for the leaching of iron oxides in diasporic bauxite from the Parnassus-Giona Zone (Greece) by hydrochloric acid. Hydrometallurgy 19:259–266. https://doi.org/10.1016/0304-386X(87)90010-7

Publisher's Note Springer Nature remains neutral with regard to jurisdictional claims in published maps and institutional affiliations.